applied sciences

MDPI

Article

Synthesis of Configurable Voltage-Mode Biquads via Augmented NAM Expansion and Symbolic Mapping

Hung-Cuong Thai [1,2], Ta-Chi Jeang [1], Dedi Kurniadi [1], Sujito [3] and Hung-Yu Wang [1,4,*]

[1] Department of Electronic Engineering, National Kaohsiung University of Science and Technology, Kaohsiung 807, Taiwan; thaihungcuong@gmail.com (H.-C.T.); ching5320@gmail.com (T.-C.J.); dedikurniadi@pnp.ac.id (D.K.)
[2] Faculty of Engineering, Dong Nai Technology University, Dong Nai 76000, Vietnam
[3] Department of Electrical and Informatics Engineering, Faculty of Engineering, State University of Malang, Malang 65145, Indonesia; sujito.ft@um.ac.id
[4] PhD Program in Biomedical Engineering, Kaohsiung Medical University, Kaohsiung 807, Taiwan
* Correspondence: hywang@nkust.edu.tw; Tel.: +886-7-3814526 (ext. 15640)

Abstract

A systematic synthesis framework based on augmented nodal admittance matrix expansion and symbolic mapping for configurable voltage-mode biquadratic filters that guarantee orthogonal control over the quality factor and pole frequency is presented. The methodology builds upon an established denominator polynomial to ensure high selectivity stability and easy adjustment of filter parameters. By formulating an augmented 3×3 core admittance matrix embedded with two symbolic control variables, the proposed framework can be used to derive various filtering functions by using nodal admittance matrix expansion technique. The low-pass, high-pass, band-pass, notch, and all-pass responses are systematically extracted from this single hardware core with five input and two output voltage ports. Since the pole-generating matrix core remains completely invariant, the orthogonal parameter tunability of the active network is preserved for all extracted filter types. These synthesized filter functions are realized with current conveyors and the non-ideality of active devices is explored. The workability of the obtained multiple-input multiple-output filter is verified through HSPICE simulations using TSMC 0.18 μm CMOS technology, demonstrating the feasibility of the proposed method.

Keywords: active filter synthesis; nodal admittance matrix expansion; orthogonal tuning; voltage-mode circuits; current conveyor

Check for updates

Academic Editor: Alessandro Lo Schiavo

Received: 8 September 2026
Revised: 8 October 2026
Accepted: 12 October 2026
Published: 15 October 2026

Copyright: © 2026 by the authors. Licensee MDPI, Basel, Switzerland. This article is an open access article distributed under the terms and conditions of the Creative Commons Attribution (CC BY) license.

1. Introduction

Systematic synthesis of active filters has long been a focal point in the design of analog signal processing systems [1,2]. In this pursuit, an essential objective is the development of configurable second-order active filters that offer orthogonal control over the quality factor and the pole frequency [3–8]. Fulfilling this requirement ensures high frequency selectivity and stability, which are critical for overcoming inherent input signal limitations and optimizing voltage-mode operations [9–12]. Among the various synthesis methodologies, the nodal admittance matrix (NAM) expansion has proven to be a powerful and mathematically robust tool. Originally proposed by Haigh et al., the symbolic NAM framework leverages limit variables and pathological elements [13], such as nullators and norators, to establish a direct correspondence between abstract mathematical formulations and physically realizable active circuit topologies [13–16]. This methodology was advanced by Saad and Soliman, who

introduced current and voltage mirror elements into the expansion process, enabling the ideal representation and systematic synthesis of many active devices [17–21].

Based on pathological framework, numerous researchers have successfully generated and optimized various filter topologies [18,20,22,23]. Soliman and Li extensively applied NAM expansion to systematically synthesize Kerwin–Huelsman–Newcomb (KHN) biquads [20,24], Two-Integrator Loop structures [21], and Tow-Thomas filter [19,22,25]. The versatility of this expansion method extends well beyond filters, facilitating the systematic generation of oscillators [26–28], floating active simulators [29,30], and OTA-based floating gyrators [31].

To specifically address the demands of orthogonal tuning and high quality-factor of filter parameters using NAM expansion, the initial core admittance matrices are subsequently expanded to synthesize functional, tunable active networks for practical applications [22,32]. However, a meticulous examination of these well-established works reveals a significant theoretical omission regarding the first phase of the synthesis procedure. While the initial admittance matrices are frequently presented and utilized in the expansion phase [32,33], the existing literature lacks a comprehensive explanation of why these specific core matrices are systematically derived from the desired transfer function denominator. The foundational mathematical mapping—from the coefficients of the polynomial denominator to the exact placement of components within the unexpanded admittance matrix—remains opaque. In most publications, the formulation of this crucial initial matrix is treated as a pre-determined given, rather than a rigorous, step-by-step mathematical procedure.

This paper aims to bridge this critical theoretical void by proposing a fully deterministic mathematical framework dedicated to the systematic construction of the initial admittance matrices for voltage-mode configurable biquadratic filters. By anchoring the synthesis on an arranged denominator, we introduce a symbolic mapping layer within an augmented 3×3 NAM. Two symbolic control variables representing the feedforward admittances injected into the network serve as steering parameters to mathematically determine the exact feedforward input excitation pathways. Rather than relying on heuristic or trial-and-error node assignments, by strategically configuring these two variables, we can extract all five standard filter responses—low-pass (LP), high-pass (HP), band-pass (BP), all-pass (AP), and notch—from a single, versatile matrix core. This work clarifies the initial matrix formulation process, providing analog designers with a clear path from a desired second-order transfer function to a structured NAM suitable for hardware realization. The feasibility is verified by simulation result of some obtained synthesized filters.

2. The Augmented NAM Synthesis Framework

In this section, the mathematical foundation of the proposed systematic synthesis procedure is described. To provide a clear, step-by-step overview of the methodology, the structural roadmap of the proposed synthesis framework is illustrated in Figure 1. Initially, a universally biquadratic denominator is adopted as the foundational core to ensure strictly orthogonal control over the filter's critical parameters. Then, an augmented NAM is formulated by integrating two symbolic variables, X and Y, into the input excitation vector. Finally, the generalized nodal voltage transfer functions are derived, establishing the required theoretical blueprint to extract various filter responses.

2.1. Formulation of the Augmented NAM Framework

In the field of high-performance active filter synthesis, the orthogonal tuning of the pole frequency (ω_0) and the quality factor (Q) is a mandatory prerequisite for ensuring high selectivity and operational stability. To fulfill these design requirements, the target second-order denominator polynomial $D(s) = s^2 + (\omega_0/Q)s + \omega_0^2$ is mapped onto the nodal admittance matrix parameters, resulting in the ideal expressions for ω_0 and Q given by:

$$\omega_0 = \frac{1}{\sqrt{R_2 R_4 C_1 C_2}} \tag{1}$$

$$Q = \frac{R_1 R_3}{(R_3 - R_1)} \sqrt{\frac{C_2}{C_1 R_2 R_4}} = \frac{1}{(G_1 - G_3)} \sqrt{\frac{G_2 G_4 C_2}{C_1}} \tag{2}$$

As evidenced by Equations (1) and (2), ω_0 is dictated exclusively by the passive component set $\{G_2, G_4, C_1, C_2\}$, whereas Q can be independently adjusted via the conductance difference $(G_1 - G_3)$. This structural decoupling ensures complete orthogonal tuning capability and enables high-Q enhancement without disturbing the pole frequency.

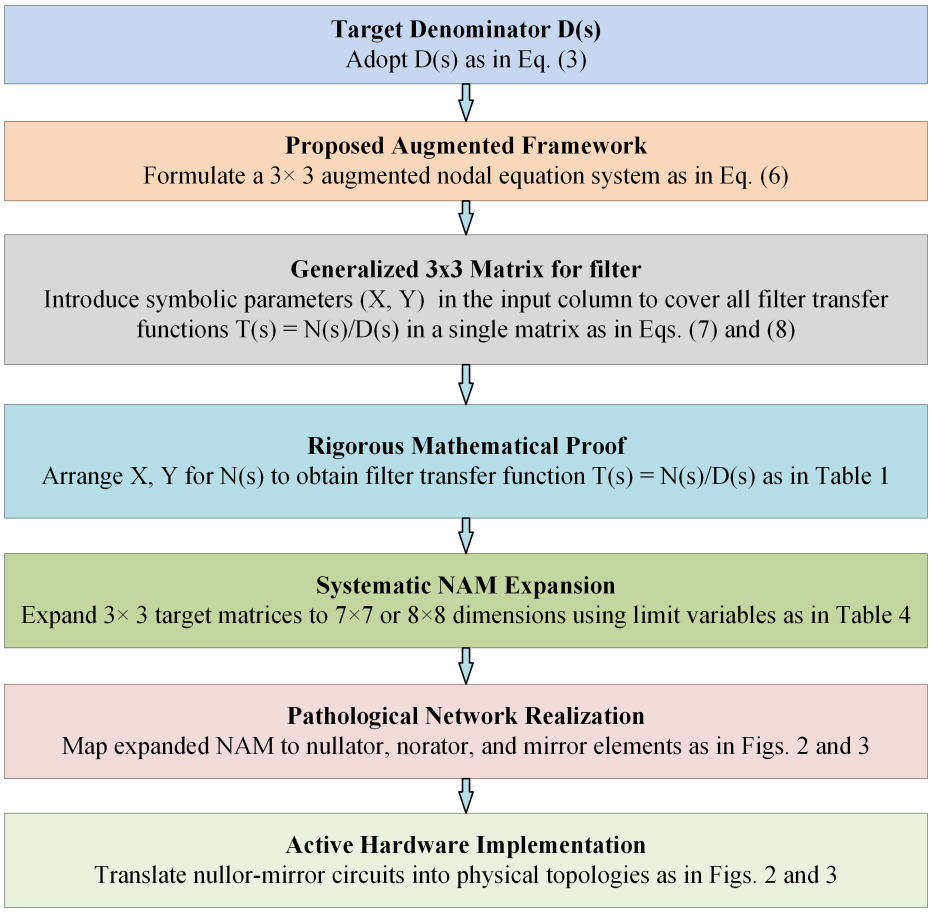


Figure 1. NAM expansion synthesis workflows of the proposed method.

To systematically satisfy this requirement, a robust strategy is to partition the synthesis process into two distinct phases: first, establishing a stable, orthogonally tunable pole generator (the denominator $D(s)$) [22,32,33] and subsequently, synthesizing the transmission zeros (the numerator $N(s)$) without disturbing the established poles.

While numerous studies have employed the general methodology of expanding various characteristic equations $D(s)$ into active networks, the specific denominator polynomial proposed by Tran et al. [32] stands out as the structurally optimal configuration for high-Q applications. It provides the mathematical feedback mechanism required to guarantee orthogonal control over Q and ω_0, and the high-Q factor can be realized without the need of large-value passive components. Consequently, the characteristic equation of this core topology for biquad is defined as Equation (3).

$$D(s) = s^2 C_1 C_2 + s C_1 (G_1 - G_3) + G_2 G_4 \tag{3}$$

According to the systematic synthesis procedures established in previous literature [32,33], this polynomial can be physically realized by mapping it into a 2×2 core admittance matrix. To satisfy the required nodal equations, the characteristic equation can be factored into two distinct physical matrix representations below.

$$Y_1 = \begin{bmatrix} sC_2 + (G_1 - G_3) & G_2 \\ -G_4 & sC_1 \end{bmatrix} \tag{4}$$

$$Y_2 = \begin{bmatrix} sC_2 + (G_1 - G_3) & -G_2 \\ G_4 & sC_1 \end{bmatrix} \tag{5}$$

While both 2×2 matrices yield the identical denominator $D(s)$ upon computing their determinants, this work adopts the configuration Y_1 in Equation (4) as the foundational pole-generating core for the subsequent synthesis steps and focuses on the implementations derived from Y_1, serving as a demonstration of the proposed theory. The same systematic procedure can be applied to the configuration Y_2 in Equation (5).

In standard active network synthesis, transitioning from a pole-generating 2×2 core to a functional voltage-mode filter requires the rigorous introduction of an external voltage excitation (V_{in}). While previous literature [32,33] successfully presented specific 3×3 matrices to realize individual filter responses, they merely assigned passive admittances to the input column without a formal mathematical explanation of their origins. The input-to-internal-node coupling was essentially treated as ad-hoc, heuristic solutions. To establish a universal framework, we formulate a 3×3 augmented nodal equation system ($[I] = [Y][V]$). Rather than relying on predefined passive admittances, we construct this system such that the established 2×2 core sub-matrix is embedded, while the input excitation pathways are explicitly controlled by two symbolic variables X and Y, representing the dynamic feedforward admittances injected into the network, as expressed in (6).

$$\begin{bmatrix} V_{in} \\ I_2 \\ I_3 \end{bmatrix} = \begin{bmatrix} 1 & 0 & 0 \\ X & sC_2 + (G_1 - G_3) & G_2 \\ Y & -G_4 & sC_1 \end{bmatrix} \begin{bmatrix} V_1 \\ V_{O1} \\ V_{O2} \end{bmatrix} \tag{6}$$

where V_{in} in Equation (6) represents the magnitude of the excitation source.

The mathematical discipline of Equation (6) yields two advantages, the first of which is rigid voltage-mode enforcement and pole stability. Following the practical voltage-mode NAM conventions established by Tran et al. [32], the first row $(1, 0, 0)$ acts as an excitation constraint that explicitly forces the input node to an ideal voltage source (V_{in}) by ensuring its nodal current remains entirely independent of the internal node voltages. It must be noted that the inputted voltage source is regarded as its R-nullor equivalent circuit [33], which establishes the voltage-mode nature of the synthesis without loading the internal nodes. The core 2×2 sub-matrix (rows 2–3, columns 2–3) remains isolated from the input parameters; consequently, the determinant of this submatrix yields the high-Q denominator $D(s)$ in Equation (3), ensuring that ω_0 and Q remain invariant regardless of the filter type being realized. The second advantage lies in the orthogonal zero manipulation. While the core pole-generating matrix is anchored in established theory, the introduction of the admittance parameters X and Y represents the primary mathematical novelty of this proposed framework. Located in the first column, these symbolic variables act on the input vector V_{in} to dictate precisely how the input voltage is converted into excitation currents injected into the internal nodes (V_{O1} and V_{O2}).

For example, by observing Table 1 and Figure 2, it can be found that R_4, and C_2 are the elements through which currents are injected from the respective input sources for

LP and HP filters, respectively. By mapping X and Y to specific symbolic admittances, the designer can arrange the desired numerator polynomial, thereby effectively decoupling the transmission zeros from the system's poles and providing a unified blueprint to extract LP, HP, BP, AP, or notch responses from a single core topology.

2.2. Generalized Transfer Functions at Nodal Ports V_{O1} and V_{O2}

The versatility of the proposed augmented NAM framework is demonstrated by deriving the explicit nodal voltage transfer functions. By setting the internal nodal currents to zero ($I_2 = I_3 = 0$) and applying Cramer's rule to the augmented matrix in Equation (6), the symbolic relationships for the output voltages at nodes V_{O1} and V_{O2} relative to the input V_{in} are formulated below.

$$\frac{V_{O1}}{V_{in}} = \frac{-XsC_1 + YG_2}{C_1C_2s^2 + sC_1(G_1 - G_3) + G_2G_4} \tag{7}$$

$$\frac{V_{O2}}{V_{in}} = \frac{-Y(sC_2 + G_1 - G_3) - XG_4}{C_1C_2s^2 + sC_1(G_1 - G_3) + G_2G_4} \tag{8}$$

Equations (7) and (8) constitute the "design blueprint" of the proposed synthesis method. The selection of the symbolic variables X and Y—whether mapped to frequency-independent conductances, capacitive terms, or hybrid admittances—enables the designer to steer the transmission zeros to desired location in the complex plane.

This nodal flexibility ensures that all five standard biquadratic functions (LP, HP, BP, AP, and notch) can be derived from a single core. Consequently, these generalized nodal equations provide the direct theoretical blueprints required for the systematic hardware realization phase in the subsequent section.

3. Systematic Realization of Filter Responses

This segment focuses on the physical implementation of the synthesized biquadratic filters. The systematic realization procedure initiates by extracting the 3×3 admittance matrix (Y) directly from the augmented nodal equation system ($[I] = [Y][V]$) formulated in Equation (6). By mapping the symbolic variables X and Y, this generalized matrix is translated into 3×3 target admittance matrices tailored for each standard filter function. Once these foundational core matrices are explicitly determined, a NAM expansion is executed to map the parameters into realizable pathological networks [22,31]. Then we demonstrate how these expanded frameworks are converted into practical hardware configurations using active building blocks.

3.1. Mapping of Symbolic Variables for Standard Filter Functions

The transition from the generalized symbolic framework to specific biquadratic responses is achieved through a strategic assignment of the control variables X and Y. By mapping these variables to specific admittance terms—such as conductances (G_i), capacitive terms (sC_i), or their hybrid combinations—the numerators of the transfer functions derived in Section 2.2 can be precisely tailored to satisfy the standard polynomial forms for LP, HP, BP, AP, and notch filters.

An inherent advantage of the proposed augmented NAM framework lies in its structural diversity, which offers analog designers significant topological flexibility. As governed by the transfer functions in Equations (7) and (8), the framework establishes two independent mathematical pathways—specifically via output nodes V_{O1} and V_{O2}—to systematically extract the desired filtering functions. This structured parameter selection guarantees that while all transmission zeros are precisely steered in the complex plane, the system's pole characteristic remain consistently anchored to the core denominator $D(s)$. On one hand,

the synthesis pathway at node V_{O1} provides a highly straightforward mapping relationship. Because the symbolic variables X and Y are explicitly decoupled in the algebraic terms of Equation (7), realizing the complete family of biquadratic filters requires only fundamental admittance assignments, as summarized in Table 1.

Table 1. Mapping of the symbolic control variables X and Y for standard biquadratic filter responses extracted at node V_{O1}.

Filter Type	X	Y	Numerator N(s)
LP	0	G_4	G_2G_4
HP	$-sC_2$	0	$s^2C_1C_2$
BP	$-(G_1-G_3)$	0	$sC_1(G_1-G_3)$
$Notch$	$-sC_2$	G_4	$s^2C_1C_2+G_2G_4$
AP	$-sC_2+G_1-G_3$	G_4	$s^2C_1C_2-sC_1(G_1-G_3)+G_2G_4$

On the other hand, to fully exploit the theoretical depth of the proposed methodology and demonstrate its capacity for generating multiple circuit variants, an alternative mapping scheme is established at node V_{O2} as detailed in Table 2. While the synthesis of basic responses, such as LP and BP filters at V_{O2}, is relatively intuitive, the realization of HP, notch, and AP responses requires a more sophisticated algebraic combination of X to achieve mathematical cancellation of the feedforward terms contributed by Y. This nodal flexibility rigorously confirms that the designer is not restricted to a single physical hardware implementation, but rather possesses the structural freedom to select the optimal configuration that best aligns with specific passive component matching or scaling constraints.

Table 2. Alternative mapping of the symbolic control variables X and Y for standard biquadratic filter responses extracted at node V_{O2}.

Filter Type	X	Y	Numerator N(s)
LP	$-G_2$	0	G_2G_4
HP	$\frac{sC_1(G_1-G_3)}{G_4}$	$-sC_1$	$s^2C_1C_2$
BP	$-sC_2$	0	sC_2G_4
$Notch$	$\frac{sC_1(G_1-G_3)-G_2G_4}{G_4}$	$-sC_1$	$s^2C_1C_2+G_2G_4$
AP	$\frac{2sC_1(G_1-G_3)-G_2G_4}{G_4}$	$-sC_1$	$s^2C_1C_2-sC_1(G_1-G_3)+G_2G_4$

3.2. Functions Formulation of the Target 3 × 3 Admittance Matrices

To synthesize the physical topologies, the symbolic parameters defined in the mapping tables must first be translated into mathematical representations. By substituting the derived values of the variables X and Y from the mapping schemes (Table 1 for node V_{O1} and Table 2 for node V_{O2}) back into the augmented matrix formulated in Equation (6), the specific 3×3 target admittance matrices for each filter function are obtained.

The core matrix in Equation (6) represents the mathematical framework for the LP, HP, BP, notch, and AP responses prior to the application of pathological stamps. The core high-Q denominator and the customized numerator terms serve as the foundational templates for the subsequent NAM expansion. Table 3 demonstrates the structural diversity of the proposed methodology. At this mathematical stage, these matrices serve as objective theoretical templates, confirming the capacity of both the V_{O1} and V_{O2} nodes to satisfy all five standard biquadratic polynomial forms. Furthermore, this comparative presentation directly highlights the algebraic simplicity of the V_{O1} synthesis pathway against the frac-

tional complexity in the V_{O2} alternative, thereby establishing a foundation for selecting the most hardware-efficient physical realizations.

Table 3. The synthesized target NAMs corresponding to the standard biquadratic filter responses extracted at nodes V_{O1} and V_{O2}.

Filter Type	Target Admittance Matrix at V_{O1}	Target Admittance Matrix at V_{O2}
LP	$\begin{bmatrix} 1 & 0 & 0 \\ 0 & sC_2+G_1-G_3 & G_2 \\ G_4 & -G_4 & sC_1 \end{bmatrix}$	$\begin{bmatrix} 1 & 0 & 0 \\ -G_2 & sC_2+G_1-G_3 & G_2 \\ 0 & -G_4 & sC_1 \end{bmatrix}$
HP	$\begin{bmatrix} 1 & 0 & 0 \\ -sC_2 & sC_2+G_1-G_3 & G_2 \\ 0 & -G_4 & sC_1 \end{bmatrix}$	$\begin{bmatrix} 1 & 0 & 0 \\ \frac{sC_1(G_1-G_3)}{G_4} & sC_2+G_1-G_3 & G_2 \\ -sC_1 & -G_4 & sC_1 \end{bmatrix}$
BP	$\begin{bmatrix} 1 & 0 & 0 \\ -(G_1-G_3) & sC_2+G_1-G_3 & G_2 \\ 0 & -G_4 & sC_1 \end{bmatrix}$	$\begin{bmatrix} 1 & 0 & 0 \\ -sC_2 & sC_2+G_1-G_3 & G_2 \\ 0 & -G_4 & sC_1 \end{bmatrix}$
Notch	$\begin{bmatrix} 1 & 0 & 0 \\ -sC_2 & sC_2+G_1-G_3 & G_2 \\ G_4 & -G_4 & sC_1 \end{bmatrix}$	$\begin{bmatrix} 1 & 0 & 0 \\ \frac{sC_1(G_1-G_3)-G_2G_4}{G_4} & sC_2+G_1-G_3 & G_2 \\ -sC_1 & -G_4 & sC_1 \end{bmatrix}$
AP	$\begin{bmatrix} 1 & 0 & 0 \\ -sC_2+G_1-G_3 & sC_2+G_1-G_3 & G_2 \\ G_4 & -G_4 & sC_1 \end{bmatrix}$	$\begin{bmatrix} 1 & 0 & 0 \\ \frac{2sC_1(G_1-G_3)-G_2G_4}{G_4} & sC_2+G_1-G_3 & G_2 \\ -sC_1 & -G_4 & sC_1 \end{bmatrix}$

3.3. Systematic NAM Expansion

To physically realize the synthesized biquadratic filter topologies, the 3×3 augmented target matrices must be expanded [19,20]. Since the diagonal and off-diagonal elements in the core 3×3 NAM contain composite admittance terms, standard matrix expansion rules using pathological limit variables (infinity-variables) are applied [14,15]. By adding blank rows and columns and injecting pathological nullor and mirror element stamps, the composite passive elements are successfully decoupled into single, physically realizable admittance branches [16,17]. This algebraic expansion process introduces essential internal nodes while preserving the network's original determinant and characteristic equation, thereby ensuring that the poles and transmission zeros remain unaffected.

For the synthesis pathway at output node V_{O1}, the core 3×3 target matrices are expanded via NAM expansion to a 7×7 dimension for the LP, HP, BP, and notch configurations. However, synthesizing the AP response at this node presents a challenge since $(X = -sC_2 + G_1 - G_3)$ contains positive and negative terms. To resolve this, the target 3×3 matrix is expanded to an 8×8 dimension, where a critical eighth auxiliary node is injected into the NAM to generate an inverted input voltage $(-V_{in})$ that drives the admittance branches corresponding to $G_1 (= 1/R_1)$ and G_3. These derived mathematical expansion models for the V_{O1} pathway are detailed in Table 4.

To demonstrate the structural versatility of the proposed framework, the matrix expansion methodology is simultaneously applied to the alternative synthesis pathway at output node V_{O2} mentioned in Section 3.1. As indicated by the target matrices in Table 3, hardware-efficient 7×7 admittance configurations are derived for the LP and BP responses, as shown in Table 5. However, expanding the HP, notch, and AP configurations at node V_{O2} would require an excessive number of pathological elements and active devices, making their physical implementation more complicated than that of the V_{O1} pathway. These expanded matrix representations in Tables 4 and 5 form the topological basis for the synthesized networks. The subsequent section demonstrates their physical realization

through pathological nullor-mirror equivalent circuits, with CCII-based topologies used for illustration.

Table 4. Expanded NAMs for the primary V_{O1} filter synthesis pathway.

Filter Types	Expanded NAM Matrix
LP	$\begin{bmatrix} 1 & 0 & 0 & 0 & 0 & 0 & 0 \\ -\infty_1 & G_4+\infty_1 & 0 & 0 & 0 & 0 & -G_4 \\ 0 & 0 & sC_2+G_1 & \infty_2 & -\infty_2 & -\infty_4 & +\infty_4 \\ 0 & 0 & -\infty_3 & sC_1 & 0 & 0 & +\infty_3 \\ 0 & 0 & 0 & -\infty_2 & G_2+\infty_2 & 0 & 0 \\ 0 & 0 & 0 & 0 & 0 & G_3+\infty_4 & -\infty_4 \\ 0 & -G_4 & -\infty_3 & 0 & 0 & 0 & G_4+\infty_3 \end{bmatrix}$
HP	$\begin{bmatrix} 1 & 0 & 0 & 0 & 0 & 0 & 0 \\ -\infty_1 & sC_2+\infty_1 & -sC_2 & 0 & 0 & 0 & 0 \\ 0 & -sC_2 & sC_2+G_1 & \infty_2 & -\infty_2 & -\infty_4 & +\infty_4 \\ 0 & 0 & -\infty_3 & sC_1 & 0 & 0 & +\infty_3 \\ 0 & 0 & 0 & -\infty_2 & G_2+\infty_2 & 0 & 0 \\ 0 & 0 & 0 & 0 & 0 & G_3+\infty_4 & -\infty_4 \\ 0 & 0 & -\infty_3 & 0 & 0 & 0 & G_4+\infty_3 \end{bmatrix}$
BP	$\begin{bmatrix} 1 & 0 & 0 & 0 & 0 & 0 & 0 \\ -\infty_1 & G_1+G_3+\infty_1 & -G_1 & 0 & -G_3 & 0 & 0 \\ 0 & -G_1 & sC_2+G_1 & \infty_2 & -\infty_2 & -\infty_4 & +\infty_4 \\ 0 & 0 & -\infty_3 & sC_1 & 0 & 0 & +\infty_3 \\ 0 & 0 & 0 & -\infty_2 & G_2+\infty_2 & 0 & 0 \\ 0 & -G_3 & 0 & 0 & 0 & G_3+\infty_4 & -\infty_4 \\ 0 & 0 & -\infty_3 & 0 & 0 & 0 & G_4+\infty_3 \end{bmatrix}$
Notch	$\begin{bmatrix} 1 & 0 & 0 & 0 & 0 & 0 & 0 \\ -\infty_1 & sC_2+G_4+\infty_1 & -sC_2 & 0 & 0 & 0 & -G_4 \\ 0 & -sC_2 & sC_2+G_1 & \infty_2 & -\infty_2 & -\infty_4 & +\infty_4 \\ 0 & 0 & -\infty_3 & sC_1 & 0 & 0 & +\infty_3 \\ 0 & 0 & 0 & -\infty_2 & G_2+\infty_2 & 0 & 0 \\ 0 & 0 & 0 & 0 & 0 & G_3+\infty_4 & -\infty_4 \\ 0 & -G_4 & -\infty_3 & 0 & 0 & 0 & G_4+\infty_3 \end{bmatrix}$
AP	$\begin{bmatrix} 1 & 0 & 0 & 0 & 0 & 0 & 0 & 0 \\ -\infty_1 & sC_2+G_4+\infty_1 & -sC_2 & 0 & 0 & 0 & -G_4 & 0 \\ 0 & -sC_2 & sC_2+G_1 & \infty_2 & -\infty_2 & -\infty_4 & +\infty_4 & -G_1 \\ 0 & 0 & -\infty_3 & sC_1 & 0 & 0 & +\infty_3 & 0 \\ 0 & 0 & 0 & -\infty_2 & G_2+\infty_2 & 0 & 0 & 0 \\ 0 & 0 & 0 & 0 & 0 & G_3+\infty_4 & -\infty_4 & -G_3 \\ 0 & -G_4 & -\infty_3 & 0 & 0 & 0 & G_4+\infty_3 & 0 \\ +\infty_5 & 0 & -G_1 & 0 & 0 & -G_3 & 0 & G_1+G_3+\infty_5 \end{bmatrix}$

Table 5. Expanded NAMs for the primary V_{O2} filter synthesis pathway.

Filter Types	Expanded NAM Matrix
LP	$\begin{bmatrix} 1 & 0 & 0 & 0 & 0 & 0 & 0 \\ -\infty_1 & G_2+\infty_1 & -sC_2 & 0 & -G_2 & 0 & 0 \\ 0 & -sC_2 & sC_2+G_1 & \infty_2 & -\infty_2 & -\infty_4 & +\infty_4 \\ 0 & 0 & -\infty_3 & sC_1 & 0 & 0 & +\infty_3 \\ 0 & -G_2 & 0 & -\infty_2 & G_2+\infty_2 & 0 & 0 \\ 0 & 0 & 0 & 0 & 0 & G_3+\infty_4 & -\infty_4 \\ 0 & 0 & -\infty_3 & 0 & 0 & 0 & G_4+\infty_3 \end{bmatrix}$
BP	$\begin{bmatrix} 1 & 0 & 0 & 0 & 0 & 0 & 0 \\ -\infty_1 & sC_2+\infty_1 & -sC_2 & 0 & 0 & 0 & 0 \\ 0 & -sC_2 & sC_2+G_1 & \infty_2 & -\infty_2 & -\infty_4 & +\infty_4 \\ 0 & 0 & -\infty_3 & sC_1 & 0 & 0 & +\infty_3 \\ 0 & 0 & 0 & -\infty_2 & G_2+\infty_2 & 0 & 0 \\ 0 & 0 & 0 & 0 & 0 & G_3+\infty_4 & -\infty_4 \\ 0 & 0 & -\infty_3 & 0 & 0 & 0 & G_4+\infty_3 \end{bmatrix}$

3.4. Hardware Realization Using Active Building Blocks

The final stage of the synthesis procedure involves the practical conversion of the nullor-mirror equivalent networks into physical topologies. As extensively documented in the literature [17,22,25], these ideal nullator, norator, and current/voltage mirror pairings serve as a universal, technology-independent platform. Although the CCII is adopted in this study for physical hardware validation, these pathological equivalent networks can be systematically mapped to various active building blocks, such as differential voltage current conveyors (DVCC) or differential difference current conveyors (DDCC). To provide a clear physical mapping process, Figure 2 shows the complete family of the five standard biquadratic filter configurations (LP, HP, BP, Notch, and AP) extracted at output node V_{O1}. The ideal pathological nullor-mirror circuits and their corresponding CCII-based physical implementations are presented side by side. Figure 3 illustrates the LP and BP nullor-mirror representations and corresponding filter configurations realized at the alternative output node V_{O2}. As the synthesis of both the V_{O1} and V_{O2} pathways follows the configurable augmented NAM framework, the resulting circuits preserve the orthogonal tunability of the core denominator.

Moreover, by combining the individual filter circuits in Figures 2 and 3, it can be observed that a multi-input-multi-output (MIMO) biquadratic filter can be obtained, as shown in Figure 4. This versatile five-input dual-output network systematically extracts all five standard filtering responses via the straightforward terminal selection protocol in Table 6.

Table 6. Input terminal excitation schemes for extracting standard biquadratic filter functions at output nodes V_{O1} and V_{O2}.

Filter Type	Input ($V_{in1}, V_{in2}, V_{in3}, V_{in4}, V_{in5}$)	Output (V_{O1}, V_{O2})
LP	$0, 0, 0, 0, V_{in}$	V_{O1}
HP	$0, V_{in}, 0, 0, 0$	V_{O1}
BP	$0, 0, V_{in}, V_{in}, 0$	V_{O1}
Notch	$0, V_{in}, 0, 0, V_{in}$	V_{O1}
AP	$0, V_{in}, -V_{in}, -V_{in}, V_{in}$	V_{O1}
LP	$V_{in}, 0, 0, 0, 0$	V_{O2}
BP	$0, V_{in}, 0, 0, 0$	V_{O2}

3.5. Non-Ideal Consideration

To evaluate the practical performance limits of the synthesized MIMO biquadratic filter, the effect of CCII non-idealities and terminal parasitic elements is considered. Accounting for the i-th non-ideal CCII in Figure 4 and assuming the circuits are working at frequencies much less than the corner frequencies of current tracking gain $\alpha_i(s)$ and voltage tracking gain $\beta_i(s)$ [34,35]. The non-ideal port relations of the i-th CCII block are characterized as:

$$\begin{bmatrix} I_{Yi} \\ V_{Xi} \\ I_{Zi+} \\ I_{Zi-} \end{bmatrix} = \begin{bmatrix} sC_{Yi} & 0 & 0 & 0 \\ \beta_i & G_{Xi} & 0 & 0 \\ 0 & \alpha_i & sC_{Zi+} + G_{Zi+} & 0 \\ 0 & -\alpha_i & 0 & sC_{Zi-} + G_{Zi-} \end{bmatrix} \begin{bmatrix} V_{Yi} \\ I_{Xi} \\ V_{Zi+} \\ V_{Zi-} \end{bmatrix} \tag{9}$$

Parasitic impedances of the CCII are expressed in Equation (9) and depicted in Figure 5. It must be noted that the dual-output CCII can be used as a single current output CCII with one Z-terminal unused. By observing the non-ideal CCII model in Figure 5 and the circuit in Figure 4, it can be found that some series input resistances (R_X) can be absorbed into the implementation of R_2 and R_3, and some C_Y and C_{Z+} can be absorbed into the implementation of C_1 to reduce the parasitic effect.

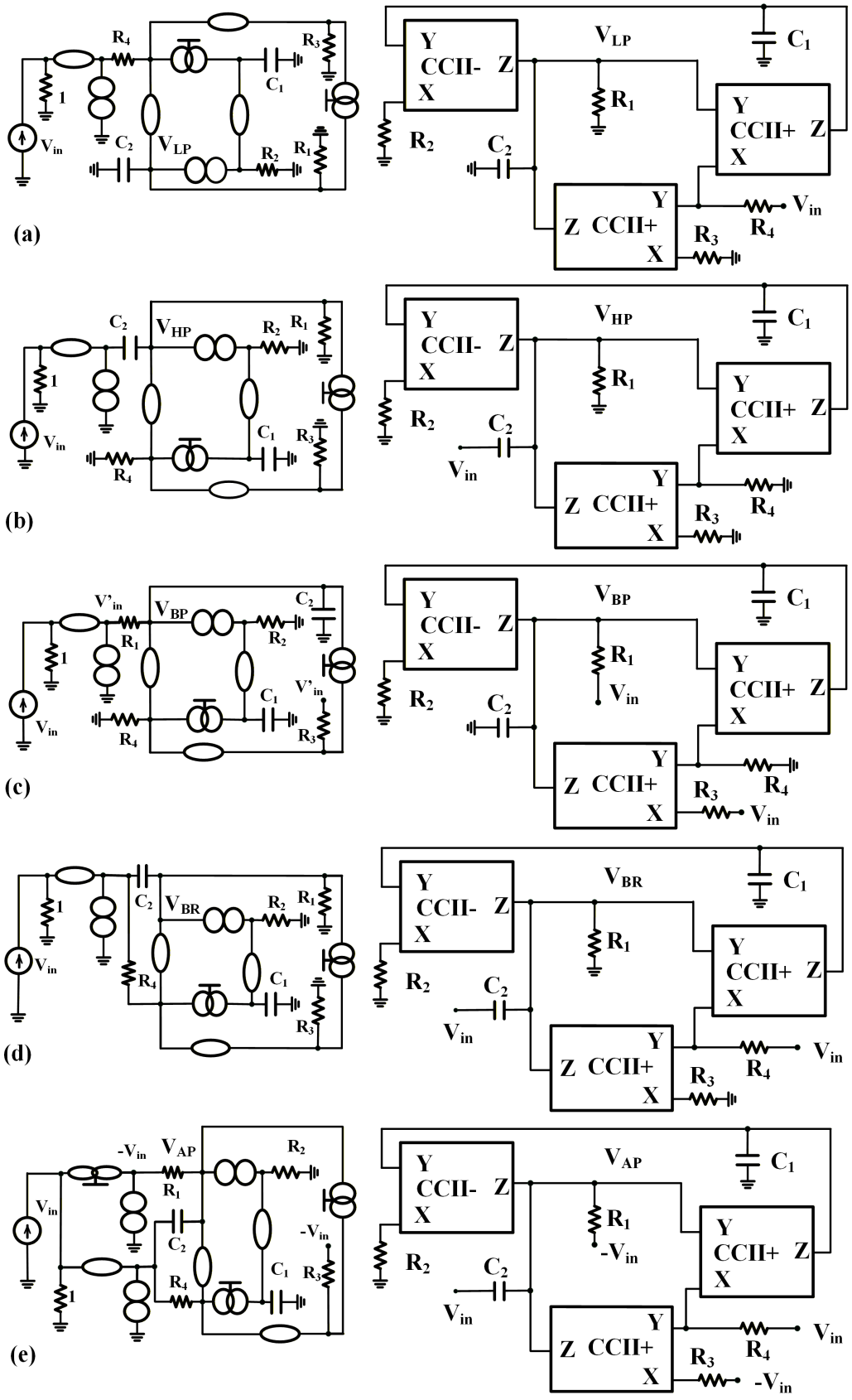


Figure 2. Synthesized filters for the primary V_{O1} pathway, showing the pathological nullor-mirror equivalent circuit (**left**) and the corresponding CCII-based active realization (**right**) for each configuration: (**a**) LP; (**b**) HP; (**c**) BP; (**d**) notch; and (**e**) AP.

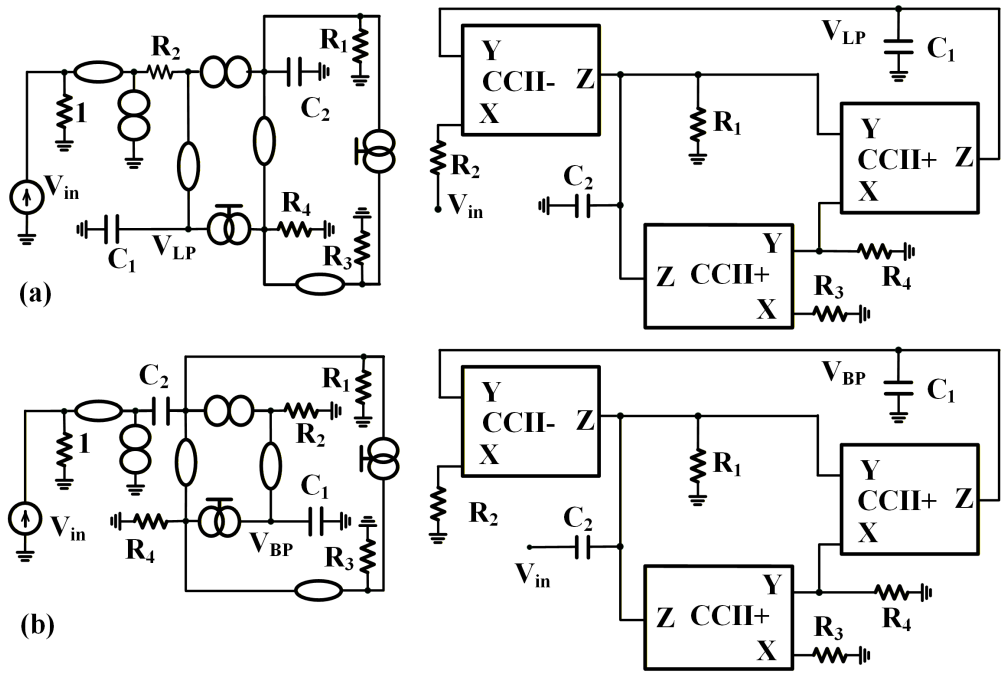


Figure 3. Synthesized filters for the alternative V_{O2} pathway, showing the pathological nullor-mirror equivalent circuit (**left**) and the corresponding CCII-based active realization (**right**) for each configuration: (**a**) LP; and (**b**) BP.

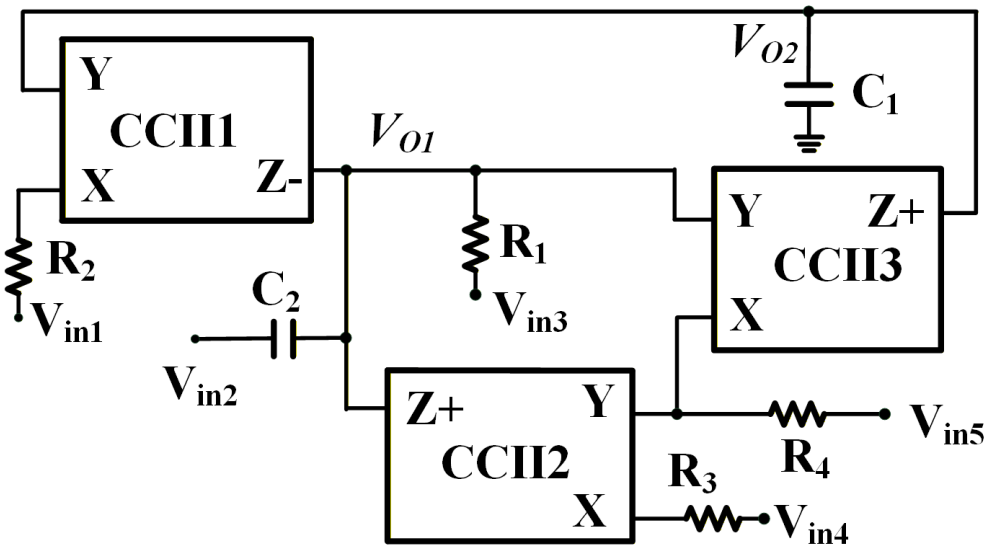


Figure 4. Circuit schematic of the proposed CCII-based MIMO voltage-mode biquadratic filter.

Taking into account the nonideal current-transfer and voltage-tracking gains shown in Figure 4, the resulting pole frequency (ω_{0n}) and quality factor (Q_n), are expressed in (10) and (11), respectively.

$$\omega_{0n} = \frac{1}{\sqrt{R_2 R_4 C_1 C_2}} \sqrt{\alpha_1 \alpha_2 \beta_1 \beta_2} \tag{10}$$

$$Q_n = \frac{R_1 R_3}{R_3 - R_1} \sqrt{\frac{C_2}{R_2 R_4 C_1}} \sqrt{\alpha_1 \alpha_2 \beta_1 \beta_2} \tag{11}$$

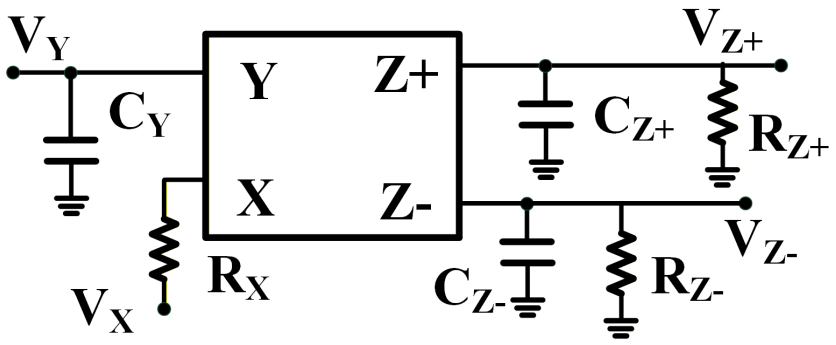


Figure 5. Parasitic impedances of the CCII.

3.6. Sensitivity Analysis

Based on Equations (10) and (11), the active and passive sensitivities can be derived in Equations (12)–(15). These expressions indicate that most sensitivities of ω_{0n} and Q_n to active and passive components are low. The passive sensitivities of Q_n with respect to the control resistors R_1 and R_3 depend solely on their resistance ratios and can be kept low through appropriate resistor selection.

$$S^{\omega_{0n}}_{\alpha_1,\alpha_2,\beta_1,\beta_2} = S^{Q_n}_{\alpha_1,\alpha_2,\beta_1,\beta_2} = S^{Q_n}_{C_2} = \frac{1}{2} \tag{12}$$

$$S^{Q_n}_{C_1,R_2,R_4} = S^{\omega_{0n}}_{C_1,C_2,R_2,R_4} = -\frac{1}{2} \tag{13}$$

$$S^{\omega_{0n}}_{R_1,R_3} = 0 \tag{14}$$

$$S^{Q_n}_{R_1} = \frac{R_3}{R_3 - R_1}, S^{Q_n}_{R_3} = -\frac{R_1}{R_3 - R_1} \tag{15}$$

4. Simulation Results and Discussions

To verify the feasibility of the proposed systematic NAM-based synthesis framework, the HSPICE simulations of derived circuit were performed with TSMC 0.18 µm CMOS model parameters. The transistor-level CMOS realization of the dual-output CCII shown in Figure 6 [36] is adopted to implement the synthesized MIMO configurable biquad. The aspect ratios of the NMOS and PMOS transistors in the CCII core are set to $W/L = 10$ µm/0.4 µm and $W/L = 5$ µm/0.4 µm, respectively. The DC supply voltages of $V_{DD} = -V_{SS} = 1$ V and the biasing voltages are $V_{B1} = -0.15$ V and $V_{B2} = -0.45$ V. To provide an evaluation of the synthesized MIMO filter architecture, several operating cases, including the universal responses at both V_{O1} and V_{O2} nodes, orthogonal Q sweeps, and independent f_0 tuning were simulated. The passive component values and the corresponding target design parameters (f_0, Q) utilized across these multi-dimensional simulation scenarios are summarized in Table 7.

Figure 7 shows the simulated magnitude responses for all five biquadratic filter configurations extracted at output node V_{O1}. The simulated frequency response for output node V_{O2} is shown in Figure 8. The response curves exhibit excellent alignment with their ideal prediction. The orthogonal adjustability of the Q without affecting the f_0 is verified via a parametric Q-sweep of the BP response at node V_{O1}. As plotted in Figures 9 and 10, the simulated result reveals the orthogonal adjustability of Q without disturbing the ω_0. The independent tunability of the pole frequency is illustrated using the notch configuration at output node V_{O1} by setting $Q = 4.67$. As depicted in Figure 11, the notch frequency is tunable by the capacitor values in Table 7.

Table 7. Component values and parameters used for the filter simulation results.

Analysis Type	f_0 (kHz) /Q	Output Node	R_1, R_2, R_3, R_4 (kΩ)	$C_1 = C_2$ (nF)
Universal (LP, HP, BP, BR, AP)	15.9/0.75	V_{O1}	5, 10, 15, 10	1
LP	15.9/0.75	V_{O2}	5, 10, 15, 10	1
BP	15.9/1	V_{O2}	6, 10, 15, 10	1
Q-Factor Sweep (BP)	15.9/3	V_{O1}	5, 10, 6, 10	1
	15.9/5.5	V_{O1}	5, 10, 5.5, 10	1
	15.9/13	V_{O1}	5, 10, 5.2, 10	1
	15.9/50.5	V_{O1}	5, 10, 5.05, 10	1
Q-Factor Sweep (LP, HP)	15.9/0.75	V_{O1}	10, 10, 15, 10	1
	15.9/1	V_{O1}	10, 10, 10, 10	1
	15.9/1.5	V_{O1}	10, 10, 7.5, 10	1
Frequency (f_0) Tuning Sweep (Notch)	1.59/4.67	V_{O1}	5, 10, 5.6, 10	10
	15.9/4.67	V_{O1}	5, 10, 5.6, 10	1
	159/4.67	V_{O1}	5, 10, 5.6, 10	0.1
	1590/4.67	V_{O1}	5, 10, 5.6, 10	0.01

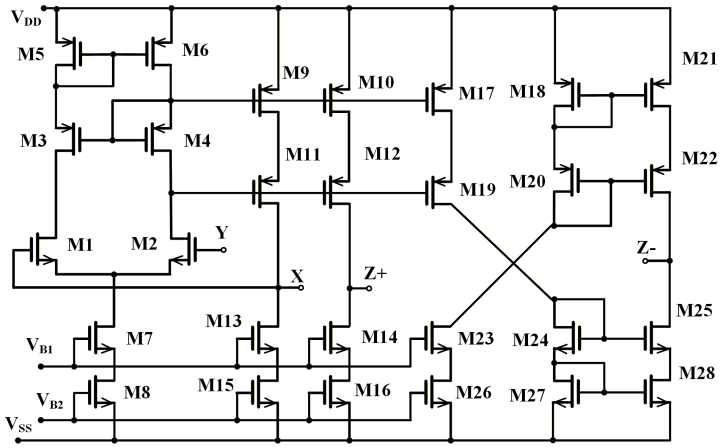


Figure 6. CMOS implementation of the CCII architecture.

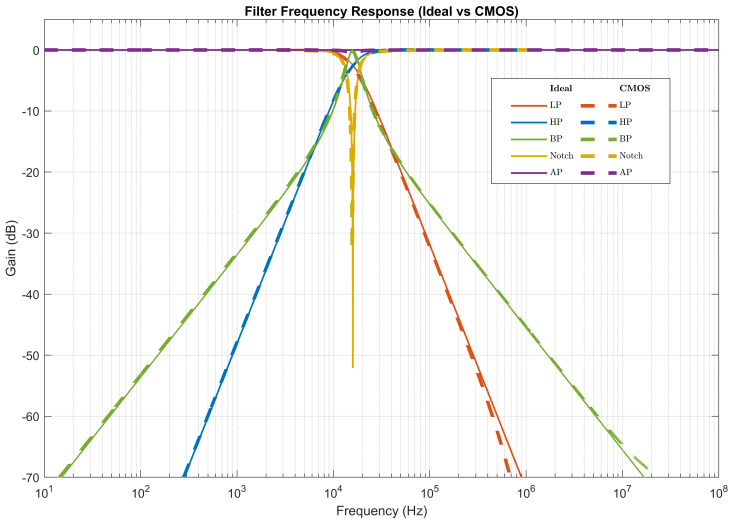


Figure 7. Simulated ideal and CMOS magnitude responses for all five synthesized standard filter configurations extracted at node V_{O1}.

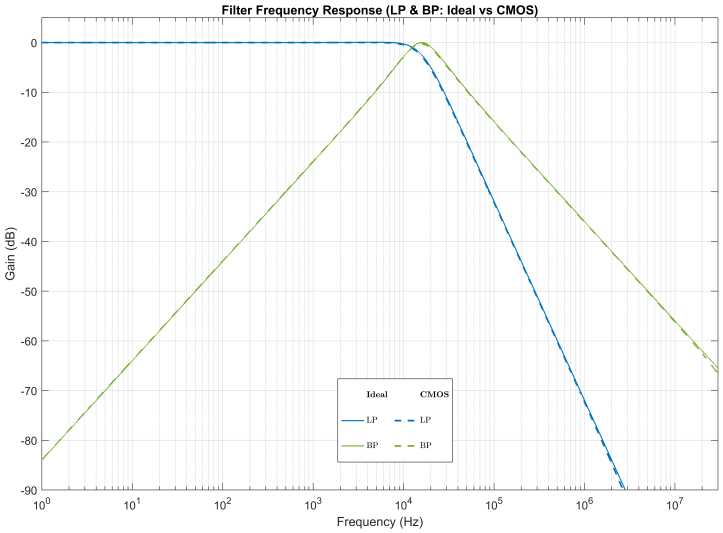


Figure 8. Simulated ideal and CMOS magnitude responses for LP and BP filter configurations extracted at node V_{O2}.

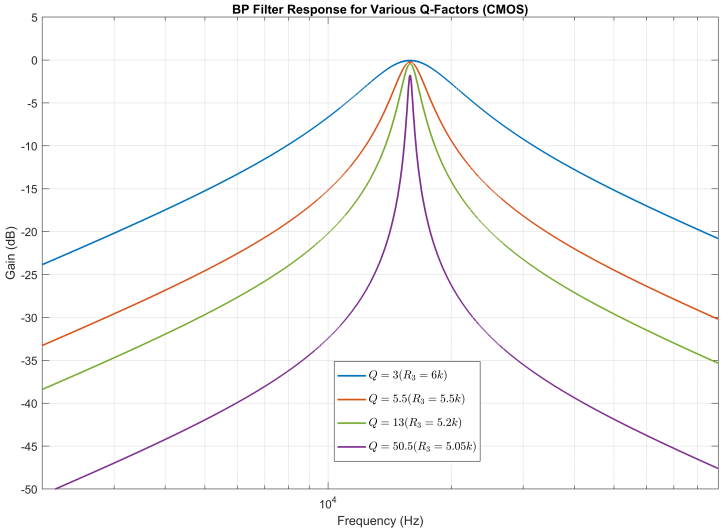


Figure 9. Simulated BP frequency responses at output node V_{O1} under Q sweeps at a fixed center frequency $f_0 = 15.9$ kHz.

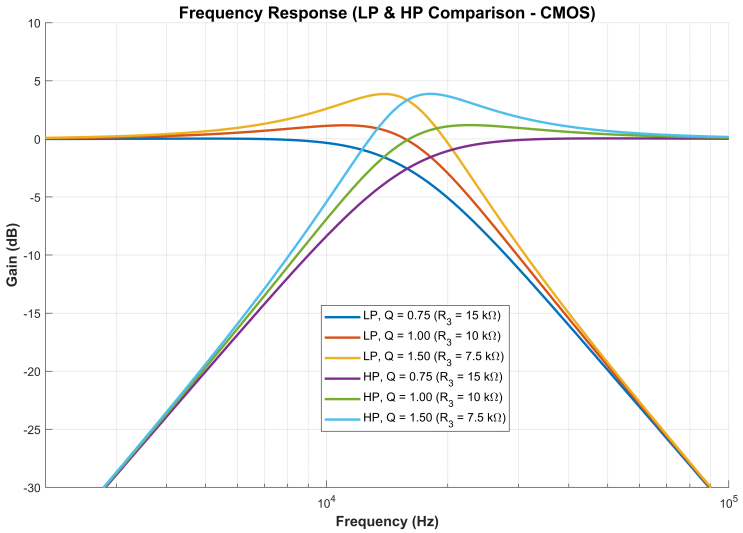


Figure 10. Simulated LP and HP magnitude responses under Q sweeps illustrating the overshoot and gain peaking characteristics near the cutoff region.

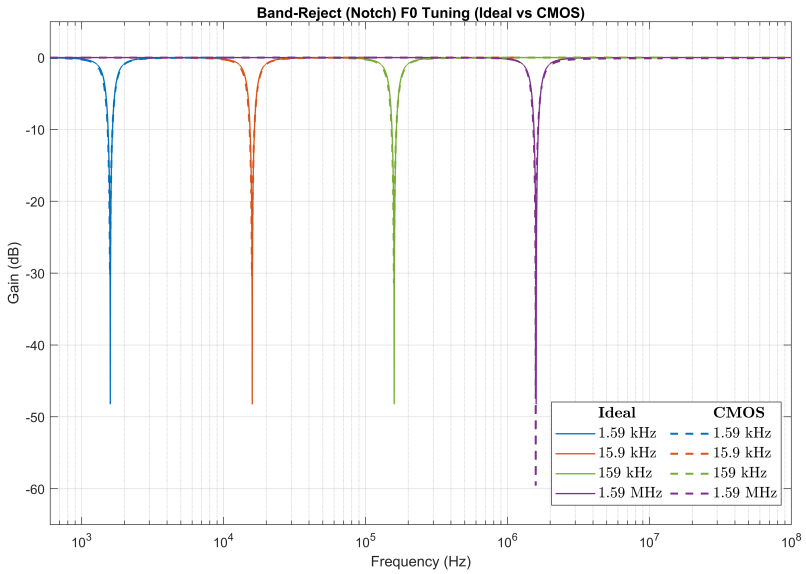


Figure 11. Simulated notch filter frequency responses at output node V_{O1} under independent f_0 tuning at a constant quality factor $Q = 4.67$.

5. Conclusions

In this paper, we presented a systematic synthesis framework for configurable voltage-mode biquad based on augmented NAM expansion and symbolic mapping. The fundamental mathematical contribution of this work lies in its deterministic mapping methodology, which utilizes two symbolic variables to precisely locate the feedforward input excitation pathways, thereby completely bypassing the heuristic trial-and-error limitations of conventional NAM expansion techniques. By mapping these control variables into an augmented 3×3 admittance core, five standard filter transfer functions are derived and used to obtain realizable nullor-mirror equivalent circuits by using NAM expansion. The physical implementations of the expanded nullor-mirror equivalent circuits are exemplified by CCII-based topologies. Since these topologies share a common hardware core, they are integrated into a MIMO filter. The functionality of the resulting filter is verified through HSPICE simulations, demonstrating the feasibility of the proposed approach.

Author Contributions: Conceptualization, H.-C.T. and H.-Y.W.; methodology, S. and H.-C.T.; theoretical verification, T.-C.J.; writing—review and editing, H.-C.T. and H.-Y.W.; project administration, D.K. and S.; funding acquisition, T.-C.J. and S. All authors have read and agreed to the published version of the manuscript.

Funding: This research was funded by the Ministry of Education of the Republic of China.

Institutional Review Board Statement: Not applicable.

Informed Consent Statement: Not applicable.

Data Availability Statement: The original contributions presented in this study are included in the article. Further inquiries can be directed at the corresponding authors.

Acknowledgments: The technical support from the Taiwan Semiconductor Research Institute is gratefully acknowledged.

Conflicts of Interest: The authors declare no conflict of interest.

References

1. Mohan, P.V.A. *Current-Mode VLSI Analog Filters*; Springer: Boston, MA, USA, 2003; ISBN 978-0-387-25134-9. [CrossRef]

2. Raut, R.; Swamy, M.N.S. *Modern Analog Filter Analysis and Design: A Practical Approach*; McGraw-Hill Education: New York, NY, USA, 2010; ISBN 978-0-07-160107-8. [CrossRef]
3. Faseehuddin, M.; Herencsar, N.; Albrni, M.A.; Shireen, S.; Sampe, J. Electronically tunable mixed mode universal filter employing grounded capacitors utilizing highly versatile VD-DVCC. *Circuit World* **2021**, *48*, 511–528. [CrossRef]
4. Jaikla, W.; Khateb, F.; Kumngern, M.; Kulej, T.; Ranjan, R.K.; Suwanjan, P. 0.5 V fully differential universal filter based on multiple input OTAs. *IEEE Access* **2020**, *8*, 187832–187839. [CrossRef]
5. Khateb, F.; Kumngern, M.; Kulej, T. 58-nW 0.5-V mixed-mode universal filter using multiple-input multiple-output OTAs. *IEEE Access* **2023**, *11*, 130345–130357. [CrossRef]
6. Kumngern, M.; Khateb, F.; Kulej, T.; Tooprakai, S. Current-mode active filter using EX-CCCII. *Electronics* **2024**, *13*, 2059. [CrossRef]
7. Shankar, C.; Khened, S.; Rai, B.K.; Khateb, F. 0.5 V BD-MIMO DDTA-based universal multimode biquad filter. *IEEE Access* **2026**, *14*, 52479–52490. [CrossRef]
8. Senani, R.; Bhaskar, D.R.; Singh, A.K. *Current Conveyors: Variant Implementations, Properties, Applications and Circuit Architectures*; Springer: Cham, Switzerland, 2015; ISBN 978-81-322-2591-1. [CrossRef]
9. Kumari, S.; Nand, D. DDCC-based MISO type voltage-mode first-order universal filter. In Proceedings of the 2022 2nd International Conference on Intelligent Technologies (CONIT), Hubli, India, 24–26 June 2022; pp. 1–6. [CrossRef]
10. Kumngern, M.; Khateb, F.; Kulej, T.; Knobnob, B. 1 V tunable high-quality universal filter using multiple-input operational transconductance amplifiers. *Sensors* **2024**, *24*, 3013. [CrossRef] [PubMed]
11. Shekhar, C.; Pandey, N.; Jain, P. Compact realization of MISO shadow filters based on DDCC. *AEU-Int. J. Electron. Commun.* **2025**, *200*, 155933. [CrossRef]
12. Grib, A.; Erdei, Z.; Turcu, M.C.; Constantin, A.; Iordache, M. Using pathological elements in analog circuit analysis and simulation. *Carpathian J. Electron. Comput. Eng.* **2020**, *13*, 1–6. [CrossRef]
13. Haigh, D.; Tan, F.; Papavassiliou, C. Systematic synthesis of active-RC circuit building-blocks. *Analog Integr. Circuits Signal Process.* **2005**, *43*, 297–315. [CrossRef]
14. Haigh, D.G. A method of transformation from symbolic transfer function to active-RC circuit by admittance matrix expansion. *IEEE Trans. Circuits Syst. I Regul. Pap.* **2006**, *53*, 2715–2728. [CrossRef]
15. Haigh, D.G.; Clarke, T.J.W.; Radmore, P.M. Symbolic framework for linear active circuits based on port equivalence using limit variables. *IEEE Trans. Circuits Syst. I Regul. Pap.* **2006**, *53*, 2011–2024. [CrossRef]
16. Haigh, D.G.; Radmore, P.M. Admittance matrix models for the nullor using limit variables and their application to circuit design. *IEEE Trans. Circuits Syst. I Regul. Pap.* **2006**, *53*, 2214–2223. [CrossRef]
17. Saad, R.A.; Soliman, A.M. A new approach for using the pathological mirror elements in the ideal representation of active devices. *Int. J. Circuit Theory Appl.* **2010**, *38*, 148–178. [CrossRef]
18. Saad, R.A.; Soliman, A.M. On the systematic synthesis of CCII-based floating simulators. *Int. J. Circuit Theory Appl.* **2010**, *38*, 935–967. [CrossRef]
19. Soliman, A.M. History and progress of the Tow Thomas bi-quadratic filter part III: Generation using NAM expansion. *J. Circuits Syst. Comput.* **2010**, *19*, 529–548. [CrossRef]
20. Soliman, A.M. Kerwin Huelsman Newcomb filter using inverting CCII. *J. Circuits Syst. Comput.* **2008**, *17*, 305–316.
21. Soliman, A.M. Two integrator loop filters: Generation using NAM expansion and review. *J. Electr. Comput. Eng.* **2010**, *2010*, 108687. [CrossRef]
22. Li, Y.-A. Systematic synthesis of high-Q T–T filters employing CCCIIs. *J. Circuits Syst. Comput.* **2017**, *26*, 1750088. [CrossRef]
23. Massi, O.; Giampiccolo, R.; Bernardini, A. Nullor-based inversion of MIMO circuital systems. *IEEE Trans. Circuits Syst. II Express Briefs* **2024**, *71*, 5054–5058. [CrossRef]
24. Li, Y.-A. On the systematic synthesis of OTA-based KHN filters. *Radioengineering* **2014**, *23*, 540–548.
25. Li, Y.-A. Systematic synthesis of OTA-based T–T filters using NAME method. *J. Circuits Syst. Comput.* **2013**, *22*, 1350002. [CrossRef]
26. Li, Y.-A. Synthesis of compact VDTA-based Wien oscillators with grounded capacitors. *AEU-Int. J. Electron. Commun.* **2018**, *84*, 281–289. [CrossRef]
27. Soliman, A.M. Synthesis of oscillators using limit variables and NAM expansion. *Act. Passiv. Electron. Compon.* **2011**, *2011*, 131546. [CrossRef]
28. Faseehuddin, M.; Sivagami, P.; Shireen, S.; Tangsrirat, W. Truly mixed-mode universal filter capable of operation in MISO and SIMO configurations with quadrature oscillator as an application. *Circuits Syst. Signal Process.* **2025**, *45*, 74–115. [CrossRef]
29. Li, Y. NAM expansion method for systematic synthesis of floating gyrators using CCCCTAs. *Analog Integr. Circuits Signal Process.* **2015**, *82*, 733–743. [CrossRef]
30. Tarunkumar, H.; Shantikumar Singh, Y.; Ranjan, A. An active inductor employing a new four terminal floating nullor transconductance amplifier (FTFNTA). *Int. J. Electron.* **2019**, *107*, 683–702. [CrossRef]
31. Li, Y.-A. NAM expansion method for systematic synthesis of OTA-based floating gyrators. *AEU-Int. J. Electron. Commun.* **2013**, *67*, 289–294. [CrossRef]

32. Tran, H.-D.; Wang, H.-Y.; Nguyen, Q.-M.; Chiang, N.-H.; Lin, W.-C.; Lee, T.-F. High-Q biquadratic notch filter synthesis using nodal admittance matrix expansion. *AEU-Int. J. Electron. Commun.* **2015**, *69*, 981–987. [CrossRef]
33. Tran, H.-D.; Wang, H.-Y.; Shieh, C.-S.; Lin, M.-C.; Lin, S.-H. Tunable voltage-mode bandpass biquad synthesis using NAM expansion method. *J. Circuits Syst. Comput.* **2016**, *25*, 1650048. [CrossRef]
34. Horng, J.-W.; Hou, C.-L.; Chang, C.-M.; Chung, W.-Y.; Wei, H.-Y. Voltage-mode universal biquadratic filters with one input and five outputs using MOCCIIs. *Comput. Electr. Eng.* **2005**, *31*, 190–202. [CrossRef]
35. Unuk, T. A current-mode universal filter with CCIIs. *J. Circuits Syst. Comput.* **2026**. [CrossRef]
36. Acar, C.; Kuntman, H. Limitations on input signal level in voltage-mode active-RC filters using current conveyors. *Microelectron. J.* **1999**, *30*, 69–76. [CrossRef]

Disclaimer/Publisher's Note: The statements, opinions and data contained in all publications are solely those of the individual author(s) and contributor(s) and not of MDPI and/or the editor(s). MDPI and/or the editor(s) disclaim responsibility for any injury to people or property resulting from any ideas, methods, instructions or products referred to in the content.